

A Novel Technique for Measuring Cycle-Resolved Cold Start Emissions applied to a Gasoline Direct Injection Engine

Jinghu Hu, Matthew Hall, and Ron Matthews University of Texas - Austin

Peter Moilanen, Steven Wooldridge, and Jianwen Yi Ford Motor Company

Abstract

There is keen interest in understanding the origins of engine-out unburned hydrocarbons emitted during SI engine cold start. This is especially true for the first few firing cycles, which can contribute disproportionately to the total emissions measured over standard drive cycles such as the US Federal Test Procedure (FTP). This study reports on the development of a novel methodology for capturing and quantifying unburned hydrocarbon emissions (HC), CO, and CO₂ on a cycle-by-cycle basis during an engine cold start. The method was demonstrated by applying it to a 4 cylinder 2 liter GTDI (Gasoline Turbocharged Direct Injection) engine for cold start conditions at an ambient temperature of 22°C. For this technique, the entirety of the engine exhaust gas was captured for a predetermined number of firing cycles. By capturing the exhaust of different numbers of firing cycles, from one to five for example, the emissions contribution of each successive cycle was determined on an ensemble average basis. The development of custom engine control software allowed predetermined event-by event control of individual cylinder fuel injection and spark settings. A dual injection strategy was studied with both an early and a late injection. Emitted masses of HCs (on a C₃ propane basis), CO and CO₂ were measured for each successive cycle. It was found that the first two firing cycle out of five contributed the most unburned hydrocarbon and CO mass, with emissions decreasing for later cycles. Measured cycle-resolved HC mass decreased monotonically from approximately 35 mg for the first firing cycle to less than 5 mg for the 5th cycle, an inordinately high value potentially due to misfires at the first two firing events. Cycle-resolved CO masses were on the order of approximately 15 mg per cycle. An advantage of the technique is that is not subject to some of the possible sampling issues that may be encountered with the use of a modal approach (i.e., fast FID + mass flow estimation) and allows the cycle-resolved quantification of CO and CO₂ mass quantities in addition to HC mass.

Introduction

There has been a huge reduction in tailpipe criteria emissions since regulations were first implemented in the mid-70's. Current U.S. Tier 3/LEVIII regulations mandate a fleet average of 30 mg/mile NMOG+NO_x by the year 2025. The criteria emissions generated during the cold start become a larger percentage of the overall emissions.

The motor vehicle industry has been compelled to implement more environmental-friendly technologies to improve the fuel economy and decrease emissions. Gasoline direct injection (GDI) engines are one of the techniques widely integrated. Compared with traditional port fuel injection (PFI) engines, fuel is directly injected into the

engine cylinders, eliminating fuel puddling and time lag [1], reducing fuel requirements and achieving higher fuel economy. Also, direct injection of fuel allows for leaner combustion limits and more accurate cycle-by-cycle injection control during open-loop operation. The charge temperature in GDI engines, due to in-cylinder evaporation of fuel, is usually lower than PFI engines, resulting in better knock resistance [2]. Offering those advantages in emission control and fuel economy, GDI engines are being rapidly deployed in the car industry. In model year 2008, GDI engines were found in fewer than 3% of the total vehicles. As of 2019, more than 50% of light-duty SI engine vehicles on the U.S. market have GDI engines [3].

Despite these advantages, one technical challenge GDI engine combustion systems still face is cold-start HC emissions [4], which is now a main focus of research. The HC mass emitted during cold-start is a major contribution to the total HC emissions for the entire EPA FTP75 driving cycle. Multiple factors contribute to high HC emission during GDI cold start. At the beginning of the cold start, the high-pressure fuel pump, driven by the extra cam lobe on the camshaft, pumps fuel into the common fuel rail to increase the fuel pressure as the engine starts cranking. The fuel rail pressure (FRP) is lower than normal working pressure (typically 35 to 200 bar) for the first few cycles [5]. The time it takes to bring the fuel rail up to working pressure strongly affects the first few firing events, influences the injection strategy and directly impacts engine start times. Optimal mixture formation is further compromised by lower cylinder wall temperature than normal steady state operation. In addition, the engine cranking speed is transient and low compared with usual operating speeds. The low fuel pressure, low cylinder wall temperature and the low engine speed all lead to unfavorable fuel vaporization and mixture preparation during cold-start [6]. The fuel tends to form a fuel film near the wall which contributes to the unburnt hydrocarbons in engine-out emissions. Besides, over-fueling during the first few events is typical to avoid misfire due to varying operating conditions and fuel volatility, which otherwise increases carbon emissions. Another possible factor for the high HC contribution for the first few cycles is that the fuel tends to be absorbed into the oil layer before combustion takes place and gets desorbed and returned to the bulk gases once the combustion finishes [7]. One strategy to improve cold start stability and reduce unburnt HC emissions is to apply split injection strategies which inject in both the intake stroke and the compression stroke [8]. Still, a more refined approach can lead to better control of the cumulative unburnt HC emission for the first few firing cycles.

During an engine cold start, the three-way catalyst (TWC) downstream in the exhaust system is inactive due to lower than optimal temperature. The low efficiency of TWC due to insufficient temperature increases the need for engine-out emission reduction,

and hence has become another challenge worthy of considering, especially for GTDI engines with turbochargers[9]. The strategies to reduce TWC light-off time and achieve fast closed-loop feedback control include spark ignition retardation[10]. Nevertheless, the overall engine combustion fueling and ignition strategy optimization is still open to study.

There has been experimental and simulation research focusing on the early stages of the cold start. Cumulative cycle quantification method was used by Imatake et.al. in PFI wall wetting research[11]. Fan et.al. studied the influence of a series of injection parameters on the engine-out emissions for the first cycle [12] and over a complete cranking process [13] based on total stoichiometric ratio and a locally rich strategy. Rodriguez and Cheng examined effects of a series of operating parameters on the engine output and engine-out emissions for the first one[7] and three firing cycles [14]. They also studied the influence of valve timing on the engine emissions during cold crank start [15]. Titus et.al. [16] studied the influence of different TWC heating strategies on the emissions. Kim et. al. used 3D CFD simulation methods to analyze engine operation with different injection timings. Malaguti et. al. used CFD methods to analyze the fuel evaporation and fuel film formation process in the first [17] and second firing cycles [18].

The first five firing cycles of the cold start process are of utmost importance. On the one hand, the first five firing cycles have the lowest engine speed, system temperature and fuel pressure, thus are most vulnerable to under-performance, misfiring and excessive emissions. On the other hand, the engine performance in the first five firing cycles plays an important role in determining the firing status of following cycles [19]. The goal of this study was to develop a technique to isolate the emissions in the first five cycles, and quantify the emission contributions to the HC, carbon monoxide (CO) and carbon dioxide (CO₂). The initial conditions were the same for each cold start test so the results are reported as ensemble averages of several tests with the assumption that the cycle-by-cycle behavior would be similar among the tests. Collecting cumulative emission data for the first five cycles will not only allow for a quantitative analysis on the cumulative emissions, but also allow for further identification of the emissions contribution of each individual firing cycle.

Experimental Methodology

A novel approach was developed to measure the engine cold-start emissions. A standard technique used to measure the highly transient HC emissions during cold-start is to use a fast FID combined with a degree resolved estimate of mass flow. This has been successfully employed in previous studies, but great care must be taken to get representative mass concentration samples. It is a transient measurement that can result in uncertainties in the phasing of the measurements associated with the transit time between the sample collection port and the analyzer. Also, since only a small portion of the exhaust flow is sampled, inhomogeneities in the species concentrations in the engine cylinders and exhaust port can lead to non-representative measured species concentrations. Non-uniform temperatures in the exhaust could also bias these measurement through its effect on gas density. And then there is the unsteady nature of the cylinder blowdown process and variable exhaust gas velocities, in general.

The approach taken in this study was to combine precise custom control of the engine fuel injection and spark processes on a cycle-

by-cycle basis and cylinder-by-cylinder basis with a technique that allowed us to capture all of the engine exhaust gas for post-analysis.

Engine Specifications

The cold-start experiments were carried out using a 2017 model-year 4-cylinder, 2 liter GTDI engine. The variable valve timing (VVT) function was disabled in the engine and default engine intake/exhaust valve timing (i.e., intake at full retard and exhaust at full advance) was maintained throughout the entire experiment. More detailed engine specifications are shown in Table 1.

Table 1 Specifications for 2.0 Liter GTDI Engine

Displacement	1999 cc
Bore/Stroke	87.5 mm/83.1 mm
Connecting Rod Length (Center to Center)	155.9 mm
Compression Ratio	9.3:1
I/O/IVC	10.9° ATDC/71.1 ABDC
EVO/EVC	55.1° BBDC/5.1 ATDC
Firing order	1-3-4-2

Experiment Setup

The experimental schematic diagram is shown in Figure 1, along with a photo of the experimental setup in Figure 2. The engine cold-start experiments were carried out in an environmental chamber, where the temperature was precisely controlled. The engine control unit (ECU) was gutted and used as a junction box to connect to both a Tektronix TBS-2000 4-channel oscilloscope and a National Instruments cRIO NI-9048 chassis, on which 7 cRIO modules were installed. The cRIO chassis was connected to the PC and controlled by in-house custom developed NI LabVIEW Real-time and FPGA control software. Fuel was provided to the engine by an external fuel system including an external fuel tank, fuel filter and an external low-pressure fuel pump. The engine was not connected to an engine dynamometer, thus no load could be applied to the engine.

Exhaust Gas Analysis Technique

A two-way exhaust pipe system was connected to the engine exhaust manifold that allowed the flow of exhaust gases to be directed either to the building exhaust system, or by the turn of a pair of gate valves, to the exhaust gas collection system. This consisted of a 1 m tall, 19 cm inner-diameter acrylic cylinder. A sliding 19 cm diameter plastic foam piston sealed the cylinder. A Horiba MEXA-554JU gas analyzer was connected to the bottom of the cylinder through a 3/8" NPT pipe fitting with a ball valve. During a cold start experiment, the entirety of the engine exhaust gas would be directed into the cylinder, raising the foam piston. After the exhaust gas collection, the valve between the cylinder and the Horiba gas analyzer was opened and HC, CO and CO₂ concentrations in the exhaust gas was analyzed.

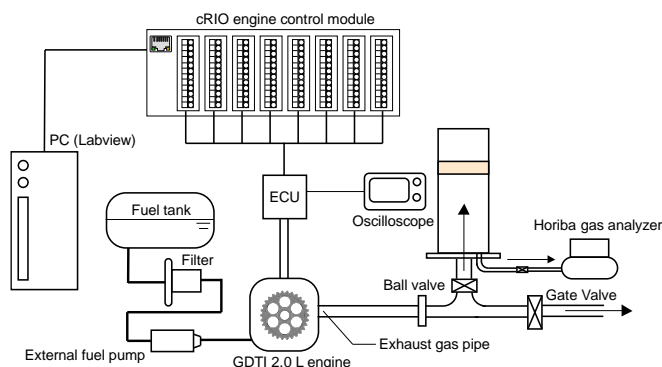


Figure 1 Schematic Diagram of the engine cold start experiment



Figure 2 Engine setup and exhaust gas collection system

Cold start experiments with the number of firing cycles ranging from 1 to 5 were carried out and emission data collected. For each firing cycle scenario, the engine was cold started by cranking the starter motor and operated with preset parameters until the targeted firing cycle number was reached. The powertrain control parameters for the injector events and spark are shown in Table 2 and the detailed timeline of the injection and spark parameters is shown in Figure 3. The control algorithms developed read the crank and cam position sensor signals to achieve engine position tracking synchronization. For the engine position tracking module, the crank angle degrees (CAD) ranged between 0 to 720 degrees for a 4-cylinder, 4-stroke engine, with 0 degrees at TDC of the compression stroke of the first cylinder to fire. Regardless of the actual engine position at the beginning of cranking, sync was achieved when the crank- and cam-shaft signals were read and the engine rotated to the reference position of 0 CAD. A cycle count index variable was initiated after sync was achieved, and was set to increment by 1 every time the crank angle degrees reached 450. The cycle index increment rules put cylinder 2 to be the first cylinder to fire. The first firing event was set to take place at cycle index 2; the engine cycle index variable was not equal to the engine's actual firing cycle.

A double injection strategy, with one injection in intake stroke and one in the compression stroke, was used to improve the fuel evaporation status inside the cylinder, and achieve good mixture preparation for the cold engine. The first cycle injected lambda is rich of stoichiometry to provide an ignitable a/f mixture at the time of spark. Some amount of the first cycle injected fuel will not evaporate and participate in combustion. DI reduces this amount of "lost fuel" versus PFI but it is still present. The early and late injection durations in the following firing cycles were reduced to match the increasing fuel rail pressure. The cylinder 2 injection duration was set to be higher than the other cylinders since the fuel rail pressure was lower during the cylinder 2 second firing event. The spark timing was set to be 10 degrees bTDC to achieve high IMEP for the engine start, and was then retarded in the 4th and 5th firing cycles to represent a transition to catalyst heating operation.

Table 2 Injection and spark parameters for the cold start injection

Firing Cycle No.	Early Injection		Late Injection		Spark Timing (DBTDC)
	Duration (ms)	SOI (DBTDC)	Duration (ms)	EOI (DBTDC)	
1	1.7	220	1.7	45	10
2	0.95 (1.7*)	220	0.95 (1.2*)	45	10
3	0.85	220	0.85	45	10
4	0.85	220	0.85	45	-10
5	0.85	220	0.85	45	-10

*: The injection durations at 2nd firing cycle for cylinder 2

The engine high-pressure fuel pump firing timing was controlled by proportional-integral (PI) control algorithms, with the fuel rail pressure set point being 52 bar for the firing cycle index up to 2, and 160 bar starting with cycle index 3. The reason for setting the fuel rail pressure to 52 bar for the first firing cycle was it balanced sufficient pressure on first firing cycle vs engine start time. The engine throttle was fixed to have a 15-degree opening angle throughout the cold start study.

Prior to the engine start, the engine control program was given the targeted number of firing cycles, between 1 and 5. The program was designed to allow the engine to complete all the firing events within that targeted firing number for each of the four cylinders, and to then turn off the injection and spark. This level of control required the control program to be modified to control the injection and spark for each cylinder individually. Initially, the control program controlled all of the cylinders together and shut down after the requested cycle index was reached. It was realized that this resulted in an injection event for one of the cylinders at the end that was not followed by a spark to complete combustion. To rectify this, individual software cylinder controls had to be developed and implemented.

After the shutdown, the engine slowed before it fully stopped, drawing in additional air during the inertia driven rotating cycles and passing it to the gas collecting cylinder. After the piston stabilized, the height of the piston was measured and the total exhaust gas volume was calculated. The gas was then sampled by the Horiba gas analyzer to obtain the HC, CO and CO₂ volumetric concentration

from which the collected masses of these three species were calculated. The emitted HC was treated as $(C_1H_{1.87})_3$ carbon based fuel, from which the total emitted carbon mass was calculated after adjusting the HC measurements which used propane as the calibration gas. For each firing cycle scenario, 6 to 8 cold starts were done to collect adequate data samples. The engine was fully cooled down after each cold start releasing the fuel rail pressure to the typical initial cold start fuel rail pressure (~5 bar), motoring to expel HC from the previous operation and waiting for more than 50 mins in the environmental chamber before next cold start experiment. A 5-liter motoring exhaust gas was collected and residual HC concentration was measured. The measured HC mass was lower than 3 mg before next cold start operation was carried out. The environmental chamber temperature was controlled to be $22 \pm 1^\circ C$ throughout the experiments.

All four of the engine cylinders were instrumented with piezoelectric pressure transducers. Using the 4-channel oscilloscope, three of these transducers were monitored and stored along with the fuel rail pressure.

The control units based on the NI LabVIEW Real-Time module recorded other powertrain relevant variables including crank angle degree, engine RPM, manifold air pressure (MAP) and fuel rail pressure obtained via the production fuel rail pressure transducer. These data were recorded and stored for analysis.

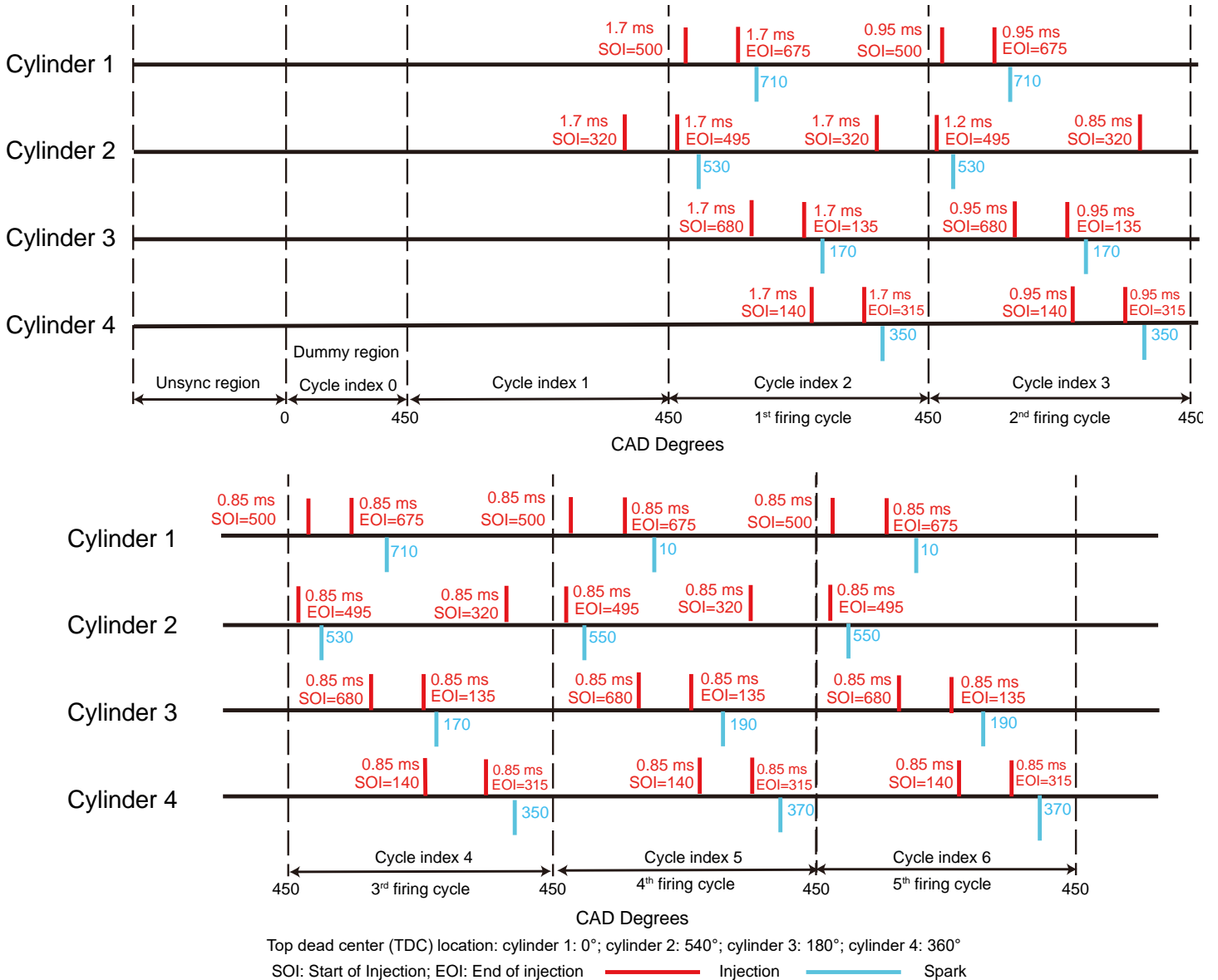


Figure 3 Preset injection and spark parameter timeline (Top is timeline through cycle 3 which continues through Cycle 5 on bottom).

Results and Discussions

An example of the cylinder pressure and fuel rail pressure data obtained via the oscilloscope for a single cold start event with 5 firing cycles is plotted in Figure 4. The engine firing order was 1-3-4-2 and the cycle index counter was preset to increment by 1 at reaching 450 crank angle degrees aTDC of compression for cylinder 1; cylinder 2 was the first to fire in a given firing cycle, followed by cylinder 1, 3 and 4. The oscilloscope trace shows the time histories of 3 cylinder pressure transducer signals and the fuel rail pressure. The first cycle, indicated by the first three pressure peaks right after $t=0$ in Figure 4, were motoring events with no injected fuel, only the high pressure pump was being controlled. The following cycle, indexed 2 or the first firing cycle, was the first cycle with complete injection and spark events. For this particular cycle, strong combustion was only observed in cylinder 3, indicating potential misfiring or weak combustion in cylinders 1 and 2. Increases in cylinder peak pressure associated with successful combustion was observed in the following

3 firing cycles. After a successful firing event the engine speed sharply increased, as shown by the smaller time gap between cycles. The following observed rapid increase in fuel rail pressure versus time resulted from both the increase in FRP set-point, and from the higher RPM that allowed higher pump volumetric efficiency and fuel flow rate. No strong cylinder peak pressures were observed in the 5th firing cycle, although it is believed that successful combustion occurred. The low peak pressures may have been caused by a decreased intake manifold air pressure, but more importantly, by the retard in the spark timing to after TDC, which caused the cylinder peak pressure to be near the motoring cylinder peak pressure. Throughout the data there were no strong combustion events, i.e., high peak pressures observed in 5th cycle. The powertrain control was shut down after the final spark event for cylinder 4, and engine would stop after going through a series of inertia cycles. The fuel rail pressure did not perfectly match the setpoint values, rather it experienced an overshoot above the setpoint then decreased to a level slightly lower than the setpoint during the rest of the cold start process.

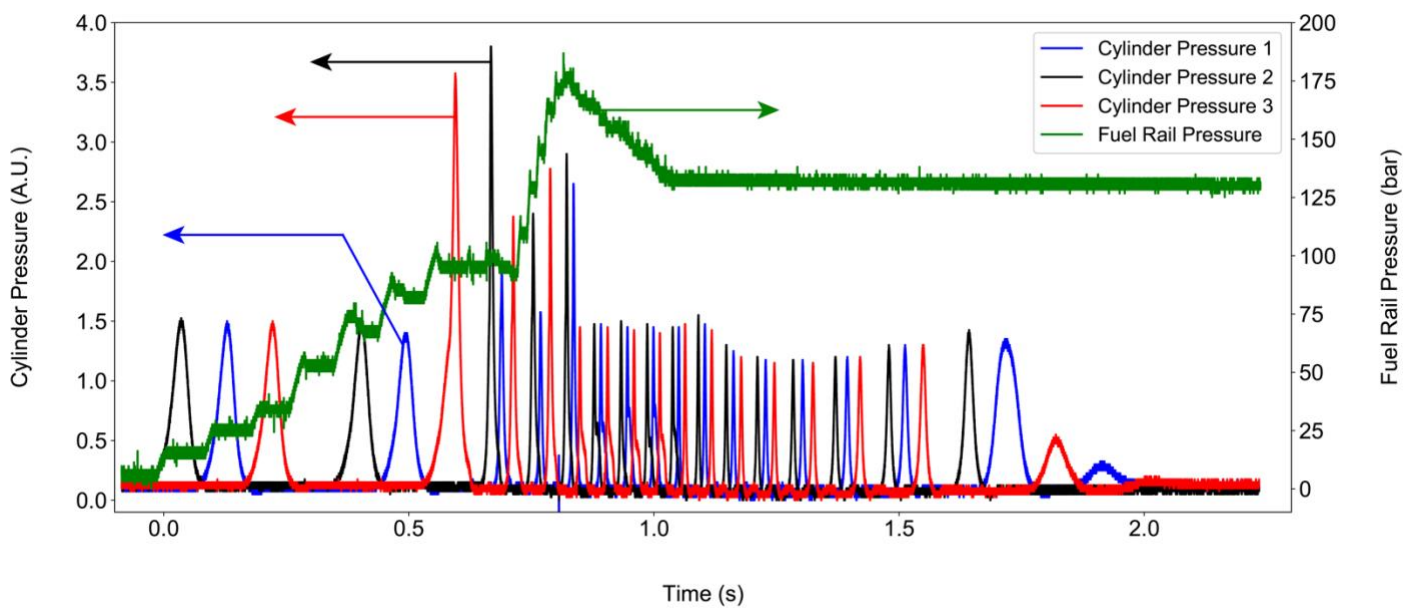


Figure 4 Cylinder pressure and fuel rail pressure data from oscilloscope

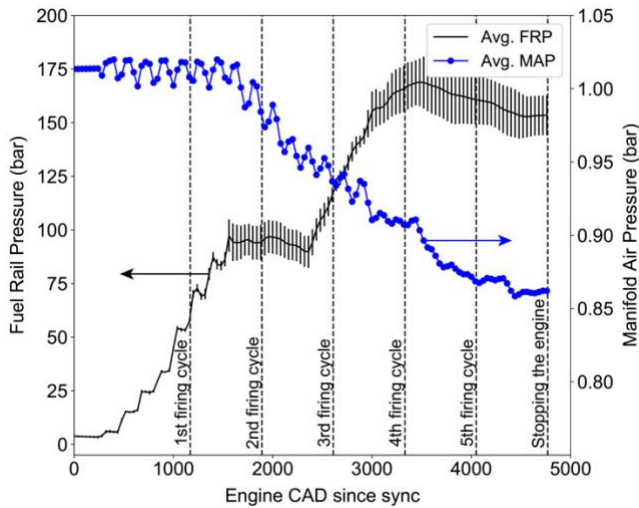


Figure 5 Average fuel rail pressure and manifold air pressure change with crank angle degree

The ensemble-averaged fuel rail pressure and intake manifold air pressure (MAP) versus crank angle degree after engine sync was obtained are shown in Figure 5. These data were obtained by averaging 5 firing cycles of FRP and MAP data. The fuel rail pressure is shown along with standard deviation as error bars. The fuel rail pressure depicted as a function of crank angle degree shows the same qualitative trends as the time-based fuel rail pressure data shown in Fig. 3. Fuel rail pressure first reached a plateau after overshooting to above the fuel rail pressure set point of 52 bar, before rising again and overshooting the setpoint of 160 bar. The MAP decreased from the beginning of the first firing cycle through the end of the last firing cycle. The decrease in MAP with each firing cycle reduced the air inducted for the later cycles, hence affecting combustion stoichiometry.

The engine control software was pre-programmed to allow two motoring cycles after engine synch was achieved and to then inject fuel and fire each of the cylinders for a set number of firing cycle 1-5. The experimental method was validated by comparing the total collected elemental carbon with the known injected carbon in the fuel. Crank angle-resolved fuel rail pressure data were obtained through the NI Real-Time control program. The data, along with the preset injection duration and timing, and the known fuel injector transfer function, was used to calculate the injected fuel mass into the cylinder. With the fuel being treated as $C_1H_{1.87}$, (typical C-H relative amounts for gasoline) the injected mass of elemental carbon was calculated. The average values of injected and collected carbon are shown in Figure 6.

The average relative difference between the collected carbon mass $m_{collected}$ and injected carbon mass $m_{injected}$, defined as,

$$\frac{m_{injected} - m_{collected}}{m_{collected}} \quad (1)$$

is shown in Figure 7.

The exhaust sampling method used in this cold start research managed to capture the majority of the elemental carbon mass

injected into the engine as fuel. The maximum difference between the measured carbon mass in the exhaust and the calculated injected fuel mass carbon was 13% in magnitude for the 1 firing cycle scenario, and reduced to 3% in magnitude for the 5 firing cycles scenario. The relative difference is negative in scenarios where 1, 2 and 4 firing cycles were allowed, and positive in scenarios where 3 and 5 firing cycles were allowed. These observed differences may reflect measurement uncertainties, but in addition, some of the injected fuel will impinge on cold combustion chamber surfaces and remain there as a “puddle”. Impingement on cylinder walls may be scraped up and reside on the piston crown and also get past the rings and end up in the sump. This may also come out in subsequent cycles as combustion chamber surfaces begin to warm. So it is possible to have a collected mass that is higher than injected.

It should be noted that post-firing inertia cycles played an important role in pushing out the emitted exhaust gas trapped in the engine gas pathway. The number of inertia cycles was small for 1 and 2 firing cycle scenarios, which probably led to the negative relative differences. As the number of firing cycles increased, the number of inertia cycles also increased, reducing the gap between the collected and injected carbon elemental mass. The positive relative difference in the 3-firing cycle scenario might be because of the rapid increase in fuel rail pressure throughout the 3rd firing cycle. The injected mass was calculated based on the fuel rail pressure at the start of the injection. The fuel rail pressure was assumed not to change significantly during the entire injection process. During the injection process in the 3rd firing cycle, fuel rail pressure increased rapidly such that the actual injected mass may have been higher than the calculated injected mass, causing the relative difference to be positive. Another important possible reason for the difference between Overall, the difference between collected and injected carbon mass was small, and the methodology used by this research was validated.

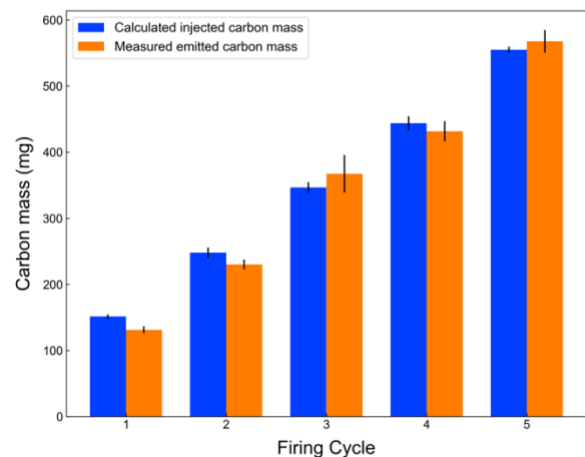


Figure 6 Injected and collected carbon mass comparison

The calculated cumulative masses of emitted HC, CO and CO₂ for different numbers of firing cycle scenarios is plotted in Figure 8. As

shown in Figure 8, the dominating carbon-based component of emission was CO₂ in all 5 firing cycles. Cumulative HC mass emission was higher than the cumulative emitted CO for the first two firing cycle scenarios, yet lower in 4 and 5 firing cycle numbers, indicating less HC generation compared with CO starting at firing cycle 3.

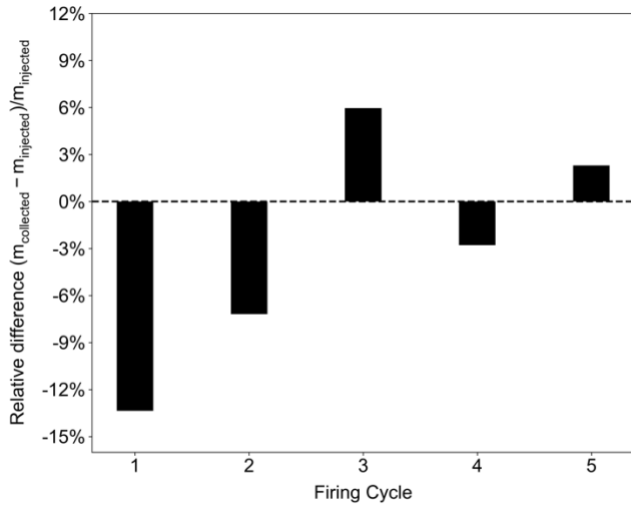


Figure 7 Relative difference between collected and injected carbon mass

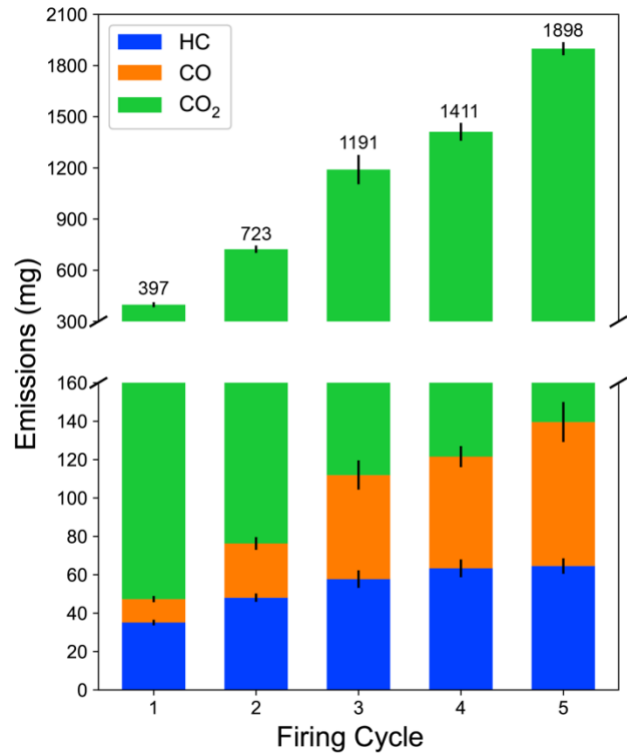


Figure 8 Emitted HC, CO and CO₂ mass for different cold start firing cycles

Aggregate data for the cold start HC, CO and CO₂ emissions for the first 5 firing cycles are plotted in Figure 9 to Figure 11. In these figures the cumulative masses are shown for each of the three emissions species along with non-cumulative (cycle resolved) mass emissions attributable to each engine cycle. The emission data collected in different cold starts for the specific firing cycle scenarios were consistent with each other, validating the repeatability of the cold start experiment. The cumulative HC emissions increased rapidly for the first three firing cycles, before reaching an average of 60 mg after the 3rd firing cycle and hardly increased in the 4th and 5th firing cycles. Looking at the cycle-resolved concentrations, HC emissions were greatest for the first two firing cycles, after which the amount of HC generation decreased approximately linearly from the 2nd to 5th firing cycles. The observed high emissions of HC in the first 2 cycles might be because of the misfiring in the first two firing events, and the reduced HC emissions in 4th and 5th firing cycle might be because of the retard in the spark ignition timing to after TDC, as some HC oxidation might occur after the EVO if spark is late enough. The observed HC generation trends were consistent with the previous literature. No obvious trends in the cycle-resolved CO and CO₂ emission were observed, except that the cycle-resolved emissions of both CO and CO₂ dropped somewhat at the 4th firing cycle. The reason for this is not entirely clear, but the rapidly decreasing MAP during this period may have temporarily reduced the exhaust flow rate preventing all of the emissions from reaching the collection cylinder. Additional and more detailed research will be necessary to further clarify these changes in cycle-resolved CO and CO₂ emissions.

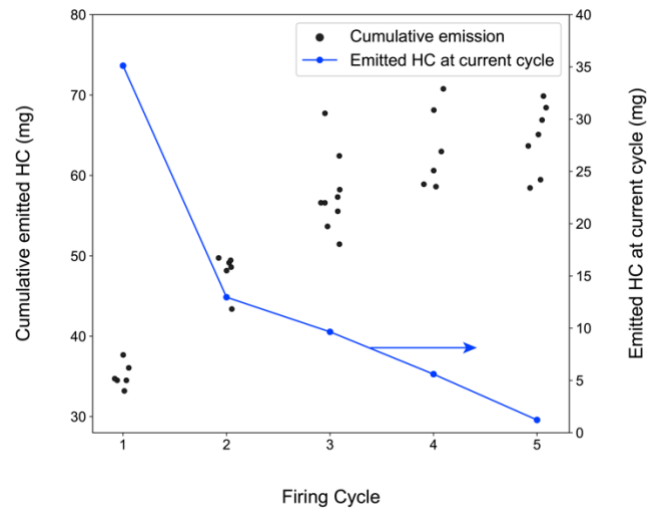


Figure 9 Current and cumulative HC emission at firing cycle 1 to 5

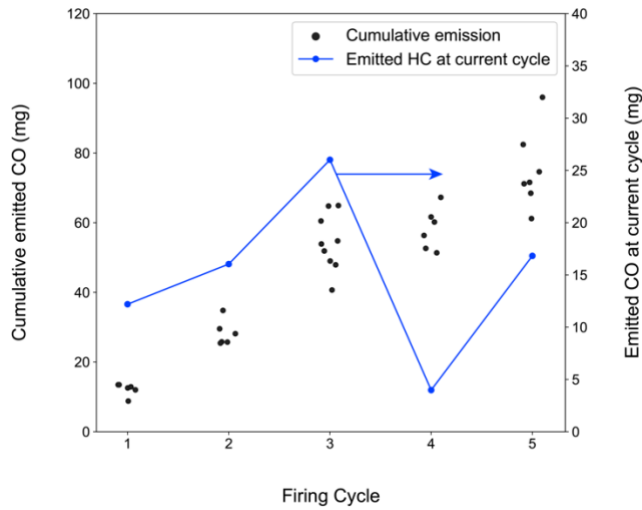


Figure 10 Current and cumulative CO emission at firing cycle 1 to 5

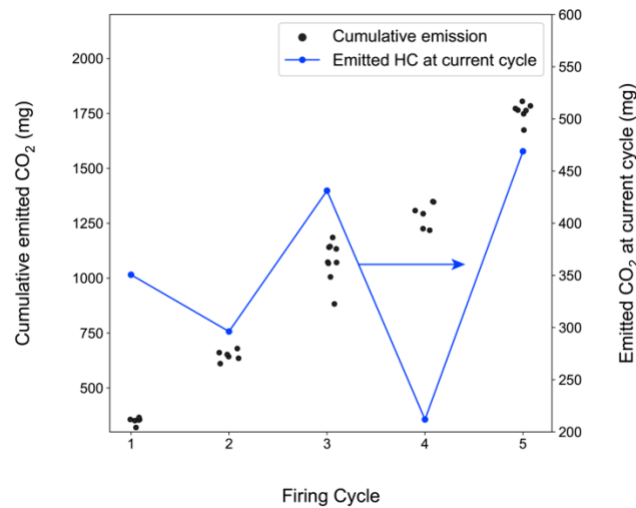


Figure 11 Current and cumulative CO₂ emission at firing cycle 1 to 5

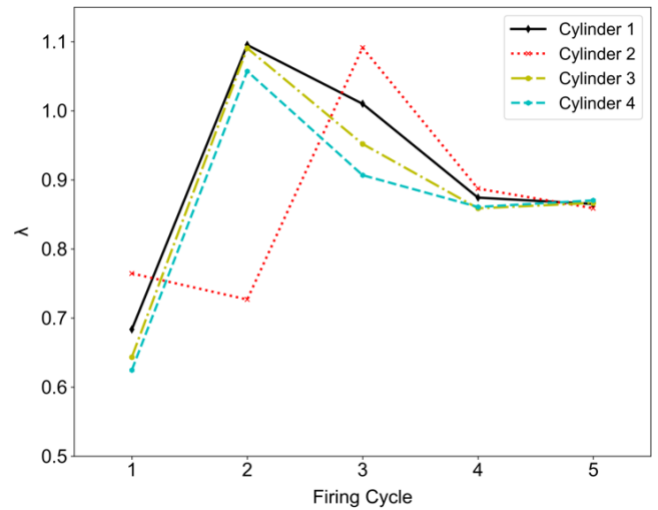


Figure 12. Average λ for firing cycle 1 to 5

The average injected air-fuel equivalence ratio (λ) for each cylinder at each firing cycle was calculated and is shown in Figure 12. The average λ values were calculated based on the calculated injected fuel mass determined by the time-resolved fuel pressure and injection duration, and the averaged air mass calculated based on the time-resolved MAP at the time of intake valve closing and the cylinder volume at that timing. The piston distance from the TDC was calculated using the following equation [20]:

$$d = \frac{S}{2} \left(1 + 2L/S - \cos(\theta_c) - \sqrt{(2L/S)^2 - \sin^2(\theta_c)} \right)$$

where d is the piston distance from the TDC, L is the connecting rod length, S is the stroke, θ_c is the crank angle degree. The cylinder pressure and volume were obtained and the intake air mass was calculated, and λ was calculated.

As the first few firing cycles of a cold start are open-loop control, non-uniform λ among the cylinders and rapidly changing AFRs were observed. For the first firing cycle, λ was low as expected due to the low initial fuel pressure. The dual injection strategy was applied to balance the need for good a/f at the spark plug while minimizing fuel impingement on the piston for the completely cold engine. Cylinders 1, 3, and 4 shared similar change in λ , while the λ trace for cylinders 2 had a unique trend. The main reason for this was because both the early and late injection durations for cylinder 2 in the 2nd firing cycle were higher than for the rest of the cylinders. The initially longer injection duration for cylinder 2 was to compensate for the lower fuel rail pressure. The result, however, was that cylinder 2 has a relatively rich burn in the 2nd firing cycle. The λ of all 4 cylinders converged by the 4th firing cycle, reaching a value of approximately $\lambda = 0.88$. Uncertainties in the injected lambda due to the control system combined with the split injection approach are likely key contributors to the observed misfire and high observed cycle 1 and 2 HC emissions.

Summary/Conclusions

A novel methodology was developed to capture and quantify the total exhaust emissions masses of unburned hydrocarbons (HCs), CO, and CO₂ for the first few firing engine cycles of a SI engine cold-start. The technique involved the captured the entirety of the engine exhaust gas for up to the first five fired engine cycles. The gases were then sampled and the emitted mass of the above exhaust species determined. The technique relied upon the development of custom engine control software that controlled the engine fuel rail pressure, fuel injection parameter and spark time on a cycle-resolved basis that additionally relied upon individual cylinder control. An advantage of the technique is that is not subject to some of the possible sampling issues that may be encountered with the use of a fast FID and allows quantification of CO and CO₂ mass quantities in addition to HC mass.

The cycle-resolved mass emissions of HCs, CO, and CO₂ were determined for the first five firing cycles for a split injection cold start scenario. This featured an intake stroke and compression stroke injection in the same cycle combined with ignition retard after the first three firing cycles.

- A mass balance that compared the collected carbon mass in the exhaust species with the calculated injected carbon mass as fuel found good agreement between the two. A difference of about 13% for the first cycle was found, but the differences found for subsequent cycles was less than 6%.
- Measured cycle-resolved HC mass decreased monotonically from approximately 35 mg for the first firing cycle to less than 5 mg for the 5th cycle. The unusually high values may have been associated with misfires indicated by measured cylinder pressure values for the first firing cycles.
- Measured cycle-resolved CO mass emissions initially increased from the first two firing cycles and then either decreased or remained approximately the same at a level of about 15 to 25 mg for the 3rd to 5th cycle. A drop, however, in both CO and CO₂ mass was observed for the 4th firing engine cycle. The reason for this is not clear, but may have been due to a reduced exhaust flow associated with the rapidly dropping intake manifold pressure or perhaps a change in species concentrations resulting from the retarded spark timing that was imposed starting with the 4th firing cycle.
- Overall, the technique shows promise for quantifying any gas-phase cold start emission species or aggregates of species, on a cycle-by-cycle basis, that are readily quantifiable with standard emissions analyzers.

References

1. Zhao, F., Lai, M.C., and Harrington, D.L., "Automotive spark-ignited direct-injection gasoline engines," *Prog. Energy Combust. Sci.* 25(5):437–562, 1999, doi:10.1016/S0360-1285(99)00004-0.
2. Queiroz, C. and Tomanik, E., "Gasoline Direct Injection Engines - A Bibliographical Review," 973113, 1997, doi:10.4271/973113.
3. The 2018 EPA Automotive Trends Report: Greenhouse Gas Emissions, Fuel Economy, and Technology since 1975, United States Environmental Protection Agency, 2019.
4. Tong, K., Quay, B.D., Zello, J.V., and Santavicca, D.A., "Fuel Volatility Effects on Mixture Preparation and Performance in a GDI Engine During Cold Start," 2001-01-3650, 2001, doi:10.4271/2001-01-3650.
5. Burke, D., Foti, D., Haller, J., and Fedor, W.J., "Fuel Rail Pressure Rise during Cold Start of a Gasoline Direct Injection Engine," 2012-01-0393, 2012, doi:10.4271/2012-01-0393.
6. Bruno, B.A., Santavicca, D.A., and Zello, J.V., "Fuel Injection Pressure Effects on the Cold Start Performance of a GDI Engine," *SAE Powertrain & Fluid Systems Conference & Exhibition*, SAE International, 2003, doi:10.4271/2003-01-3163.
7. Rodriguez, J.F. and Cheng, W.K., "Effect of Operation Strategy on First Cycle CO, HC, and PM/PN Emissions in a GDI Engine," *Sae Int. J. Engines* 8(3):1098–1106, 2015, doi:10.4271/2015-01-0887.
8. Xu, Z., Yi, J., Wooldridge, S., Reiche, D., Curtis, E.W., and Papaioannou, G., "Modeling the Cold Start of the Ford 3.5L V6 EcoBoost Engine," *SAE Int. J. Engines* 2(1):1367–1387, 2009, doi:10.4271/2009-01-1493.
9. Peckham, M.S., Finch, A., and Campbell, B., "Analysis of Transient HC, CO, NOx and CO2 Emissions from a GDI Engine using Fast Response Gas Analyzers," *SAE Int. J. Engines* 4(1):1513–1522, 2011, doi:https://doi.org/10.4271/2011-01-1227.
10. Fedor, W., Kazour, J., Haller, J., Dauer, K., and Kabasin, D., "GDI Cold Start Emission Reduction with Heated Fuel," 2016-01-0825, 2016, doi:10.4271/2016-01-0825.
11. Imatake, N., Saito, K., Morishima, S., Kudo, S., and Ohhata, A., "Quantitative Analysis of Fuel Behavior in Port-Injection Gasoline Engines," 971639, 1997, doi:10.4271/971639.
12. Fan, Q., Bian, J., Lu, H., Li, L., and Deng, J., "Effect of the fuel injection strategy on first-cycle firing and combustion characteristics during cold start in a TSDI gasoline engine," *Int. J. Automot. Technol.* 13(4):523–531, 2012, doi:10.1007/s12239-012-0050-3.
13. Fan, Q. and Li, L., "Transient Characteristics of Cold Start Emissions from a Two-Stage Direct Injection Gasoline Engines Employing the Total Stoichiometric Ratio and Local Rich Mixture Start-up Strategy," 2012-01-1068, 2012, doi:10.4271/2012-01-1068.
14. Rodriguez, J.F. and Cheng, W.K., "Cycle-by-Cycle Analysis of Cold Crank-Start in a GDI Engine," *Sae Int. J. Engines* 9(2):1210–1219, 2016, doi:10.4271/2016-01-0824.
15. Rodriguez, J.F. and Cheng, W.K., "Reduction of Cold-Start Emissions through Valve Timing in a GDI Engine," *SAE Int. J. Engines* 9(2):1220–1229, 2016, doi:10.4271/2016-01-0827.
16. Titus, F., Berlet, P., Sobek, F., and Wessling, J., "Emission Reduction during Cold Start by Combustion Controlled Increase

of In-Cylinder Temperatures,” 2018-01-1740, 2018, doi:10.4271/2018-01-1740.

Center for Efficient Vehicles and Sustainable Transportation Systems (EV-STs).

17. Malaguti, S., Cantore, G., Fontanesi, S., Lupi, R., and Rosetti, A., “CFD Investigation of Wall Wetting in a GDI Engine under Low Temperature Cranking Operations,” 2009-01-0704, 2009, doi:10.4271/2009-01-0704.
18. Malaguti, S., Fontanesi, S., and Severi, E., “Numerical Analysis of GDI Engine Cold-Start at Low Ambient Temperatures,” 2010-01-2123, 2010, doi:10.4271/2010-01-2123.
19. Yamada, T., Gardner, D.V., Bruno, B.A., Zello, J.V., and Santavicca, D.A., “The Effects of Engine Speed and Injection Pressure Transients on Gasoline Direct Injection Engine Cold Start,” 2002-01-2745, 2002, doi:10.4271/2002-01-2745.
20. Adler, U. and Bazlen, W., “Automotive Handbook,” Robert bosch GmbH, 1976.

Definitions/Abbreviations

FRP	Fuel rail pressure
GDI	Gasoline direct injection
GHG	Greenhouse gases
HC	Hydrocarbon
MAP	Manifold air pressure
PFI	Port fuel injection
TWC	Three-way catalyst

Contact Information

Prof. Matthew J. Hall
mjhall@mail.utexas.edu

The University of Texas at Austin
Department of Mechanical Engineering
204 E. Dean Keeton St. C2200
Austin, TX 78712

Acknowledgments

This project was made possible through the funding provided by the Ford Motor Co. through the University of Texas at Austin’s NSF